Technische Universität Graz

Fast Multipole Boundary Element Method for Electrostatic Field Computations

G. Of, M. Kaltenbacher, O. Steinbach

Berichte aus dem Institut für Numerische Mathematik

Bericht 2007/2

Technische Universität Graz

Fast Multipole Boundary Element Method for Electrostatic Field Computations

G. Of, M. Kaltenbacher, O. Steinbach

Berichte aus dem Institut für Numerische Mathematik

Bericht 2007/2

Technische Universität Graz
Institut für Numerische Mathematik
Steyrergasse 30
A 8010 Graz

WWW: `http://www.numerik.math.tu-graz.at`

Fast Multipole Boundary Element Method for Electrostatic Field Computations

G. Of [1], M. Kaltenbacher[2], O. Steinbach[1]

[1] Institut für Numerische Mathematik, Technische Universität Graz
Steyrergasse 30, A-8010 Graz, Austria.
{of,o.steinbach}@tugraz.at

[2] Lehrstuhl für Sensorik, Universität Erlangen–Nürnberg,
Paul–Gordan–Strasse 3/5, 91052 Erlangen, Germany.
manfred.kaltenbacher@lse.e-technik.uni-erlangen.de

Abstract

In this paper we present an efficient - both in CPU time and memory - numerical scheme for the computation of electric capacities within micromechanical transducers. Our scheme is based on solving a first kind boundary integral equation by a Galerkin Boundary Element Method (BEM). The arising linear system of equations is solved by an conjugate gradient (CG) method with an artifical Multilevel Boundary Element Preconditioner. For the matrix-vector operations within the CG-iterations we apply an appropriate Fast Multipole Method (FMM). The numerical studies demonstrate the efficiency and robustness of our computational scheme.

1 Introduction

A wide range of state-of-the-art Micro-Electro-Mechanical-Systems (MEMS) are based on the electrostatic principle, e.g. capacitive acceleration sensors, micropumps, gyro-sensors, etc. For the design of such sensors and actuators the computation of the electric capacities is of great importance. Due to the complex structure we need a numerical scheme such as the Finite Element Method (FEM) or Boundary Element Method (BEM). In most cases we are interested in the capacities as a function of all possible positions of the two electrode structures within the transducer. Therewith, a BEM, where we just have to discretize the electrode structures and not the air-regions in-between as in the case of a pure FEM, is favorable from the user's point of view. Since a BEM results in an algebraic system of equations with a fully populated system matrix, a fast BEM as first introduced in [6, 16] is needed. In addition, the iterative solution needs a preconditioning in order to guarantee convergence and to accelerate the solution process [3]. The paper is organized as follows:

In Sec. 2 we shortly discuss the physical equations and how we derive a first kind boundary element equation, which we have to solve numerically. The following section describes the application of the Galerkin Boundary Element Method, the preconditioner for the CG-solver, and the fast multipole algorithm for the evaluation of the matrix-vector operations. Finally, in Sec. 4 we present a detailed discussion on the performance of the computational scheme concerning the accuracy, the number of CG-iterations, CPU time and memory.

2 Physical Equations and Boundary Integral Equations

We consider a micromechanical transducer consisting of two bounded subdomains $\Omega_i \subset \mathbb{R}^3$ with boundaries $\Gamma_i = \partial\Omega_i$ and with given constant potentials ϕ_i, $i = 1, 2$. Our interest is an efficient computation of the capacities C_i

$$C_i \;=\; \frac{Q_i}{\phi_1 - \phi_2}, i = 1, 2 \tag{1}$$

where

$$Q_i \;=\; \varepsilon \int\limits_{\Gamma_i} \frac{\partial}{\partial n_i}\phi(x) ds_x \tag{2}$$

are the corresponding charges of the transducers and ε is the dielectric permittivity of the media between (usual air). Therefore we have to solve the exterior boundary value problem

$$-\mathrm{div}\,[\varepsilon \nabla \phi(x)] \;=\; 0 \quad \text{for } x \in \Omega^c := \mathbb{R}^3 \backslash (\overline{\Omega}_1 \cup \overline{\Omega}_2) \tag{3}$$

with given Dirichlet boundary conditions

$$\phi(x) \;=\; \phi_i \quad \text{for } x \in \Gamma_i, i = 1, 2 \tag{4}$$

and with the far field boundary condition

$$\phi(x) \;=\; \phi_0 + \mathcal{O}(\frac{1}{|x|}) \quad \text{as } |x| \to \infty. \tag{5}$$

In fact, to compute the local charges Q_i via (2) we need to have the normal derivatives $t_i = \frac{\partial}{\partial n_i}\phi$ on Γ_i, $i = 1, 2$. The solution of the exterior Dirichlet boundary value problem (3)–(5) is given by the representation formula

$$\phi(x) = \phi_0 - \int\limits_{\Gamma} U^*(x, y) t(y) ds_y + \int\limits_{\Gamma} \frac{\partial}{\partial n_y} U^*(x, y)\phi(y) ds_y$$

for $x \in \Omega^c$ where $\Gamma = \Gamma_1 \cup \Gamma_2$ and

$$U^*(x, y) \;=\; \frac{1}{4\pi}\frac{1}{|x - y|}$$

is the fundamental solution of the Laplace operator. Since $\phi(x) \equiv 1$ is a solution of the interior Laplace equation, we conclude

$$\int\limits_{\Gamma_i} \frac{\partial}{\partial n_y} U^*(x,y) ds_y \;=\; 0 \quad \text{for } x \in \mathbb{R}^3 \backslash \overline{\Omega}_i.$$

Taking the trace of the representation formula on the boundary Γ, we obtain a boundary integral equation

$$\int\limits_{\Gamma} U^*(x,y) t(y) ds_y = \phi_0 - \frac{1}{2}\phi(x) + \int\limits_{\Gamma} \frac{\partial}{\partial n_y} U^*(x,y)\phi(y) ds_y$$

for $x \in \Gamma$ almost everywhere. Using again $\phi(x) \equiv 1$, we conclude

$$\int\limits_{\Gamma_i} \frac{\partial}{\partial n_y} U^*(x,y) ds_y \;=\; -\frac{1}{2} \quad \text{for } x \in \Gamma_i$$

almost everywhere and therefore we end up with the boundary integral equation

$$\int\limits_{\Gamma} U^*(x,y) t(y) ds_y \;=\; \phi_0 - \phi_i \quad \text{for } x \in \Gamma_i, i = 1,2. \tag{6}$$

This is a first kind boundary integral equation with the single layer potential

$$(Vt)(x) \;=\; \frac{1}{4\pi} \int\limits_{\Gamma} \frac{1}{|x-y|} t(y) ds_y \quad \text{for } x \in \partial\Gamma.$$

The unique solvability of the boundary integral equation (6) follows from the ellipticity of the single layer potential V, see for example [19] for details.

3 Galerkin Boundary Element Methods

Let $S_h^\nu(\Gamma) = \text{span}\{\psi_k^\nu\}_{k=1}^N$ be a finite dimensional trial space of piecewise polynomial basis functions ψ_k^ν of polynomial degree ν which are defined with respect to an admissible and globally quasi–uniform triangulation $\Gamma_h = \cup_{i=1}^n \overline{\tau}_k$ of the boundary $\Gamma = \Gamma_1 \cup \Gamma_2$ into n plane triangular boundary elements τ_k of mesh size h. Here we will use piecewise constant basis functions ψ_k^0 with $N = n$ and piecewise linear but globally discontinuous basis functions ψ_k^1 with $N = 3n$. The Galerkin variational formulation of the boundary integral equation (6) is to find an approximate solution $t_h \in S_h^\nu(\Gamma)$ such that

$$\int\limits_{\Gamma} \psi_\ell^\nu(x) \int\limits_{\Gamma} U^*(x,y) t_h(y) ds_y ds_x = \int\limits_{\Gamma} \psi_\ell^\nu(x)[\phi_0 - \phi(x)] ds_x$$

is satisfied for all $\ell = 1, \ldots, N$. This is equivalent to a linear system of equations, $V_h^\nu \underline{t}^\nu = \underline{f}^\nu$, where the stiffness matrix V_h^ν is given by the matrix elements

$$V_h^\nu[\ell, k] \;=\; \frac{1}{4\pi} \int\limits_\Gamma \psi_\ell^\nu(x) \int\limits_\Gamma \frac{1}{|x-y|} \psi_k^\nu(y) ds_y ds_x$$

for $k, \ell = 1, \ldots, N$ while the vector of the right hand side is given by the components

$$f_\ell^\nu \;=\; \sum_{i=1}^{2} \int\limits_{\Gamma_i} \psi_\ell^\nu(x)[\phi_0 - \phi_i] ds_x, \quad \ell = 1, \ldots, N.$$

After solving the linear system $V_h^\nu \underline{t}^\nu \;=\; \underline{f}^\nu$ the corresponding approximate solution $t_h \in S_h^\nu(\Gamma)$ induces an approximate value for the capacity,

$$C_{i,h,\nu} \;=\; \frac{\varepsilon}{\phi_1 - \phi_2} \int\limits_{\Gamma_i} t_h(x) ds_x, \quad i = 1, 2.$$

Using the Aubin–Nitsche trick and assuming sufficient regularity for the exact normal derivative t one can derive an optimal error estimate, see for example [19],

$$|C_i - C_{i,h,\nu}| \;\leq\; c(\varepsilon, t)\, h^{2(\nu+1)+1}. \tag{7}$$

This error estimate shows a higher order of convergence when using piecewise linear, globally discontinuous basis functions instead of piecewise constant basis functions.

We will apply the described Galerkin boundary element method to compute the capacities of micromachined transducers. As a simple model geometry we consider transducers with two fingers per structure as given in Fig. 1.

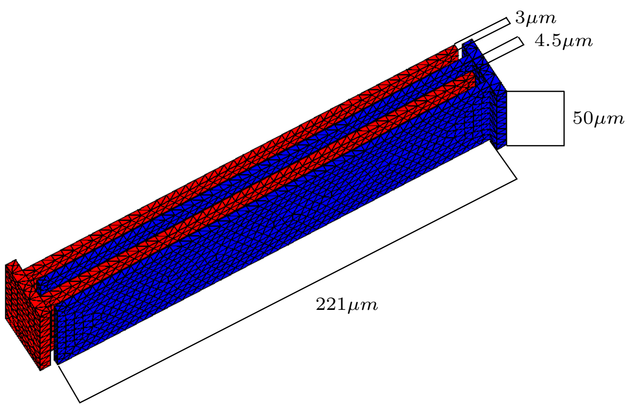

Figure 1: Geometry of a two–finger transducer.

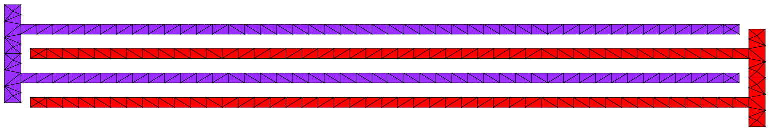

Figure 2: Centered location of the fingers.

First we assume that both transducers are centered to each other as depicted in Fig. 2. The aim is to compute the capacity of the transducers as a function of the offset in z direction. The corresponding results of these computations are given in Fig. 3 when using piecewise constant basis functions and in Fig. 4 when using piecewise linear basis functions for different boundary element discretizations.

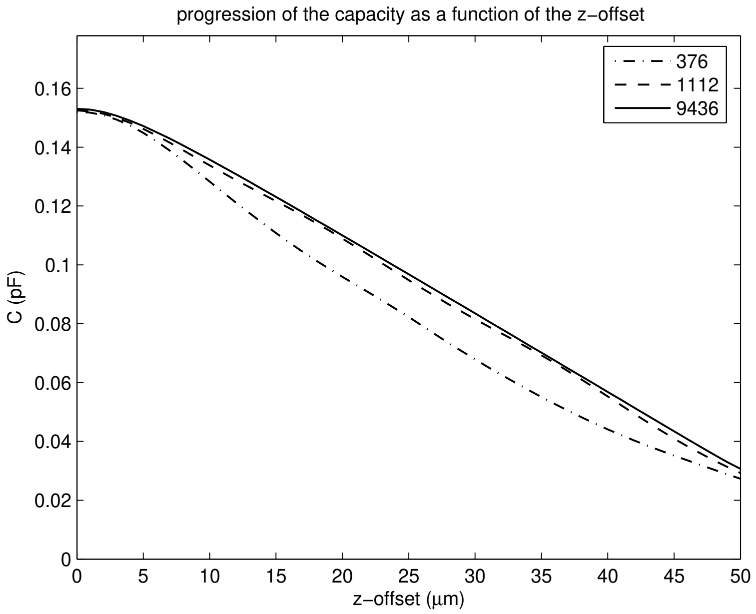

Figure 3: Capacity for centered transducers and $\nu = 0$ (piecewise constant functions).

Applying a boundary element method, we need only one triangulation of the single finger structures. In comparison, a finite element discretization of the exterior domain would require remeshings when considering different offsets in z directions.

In the standard configuration, the finger structures are centered to each other (see Fig. 2). In this situation the distance between the fingers corresponds to the thickness of the fingers themselves. Therefore a boundary element discretization of the fingers already resolves the distance. As shown in the Fig. 3 and Fig. 4, boundary element meshes of 1112 or 9436 elements give sufficiently good approximations. Note that 9436 boundary elements

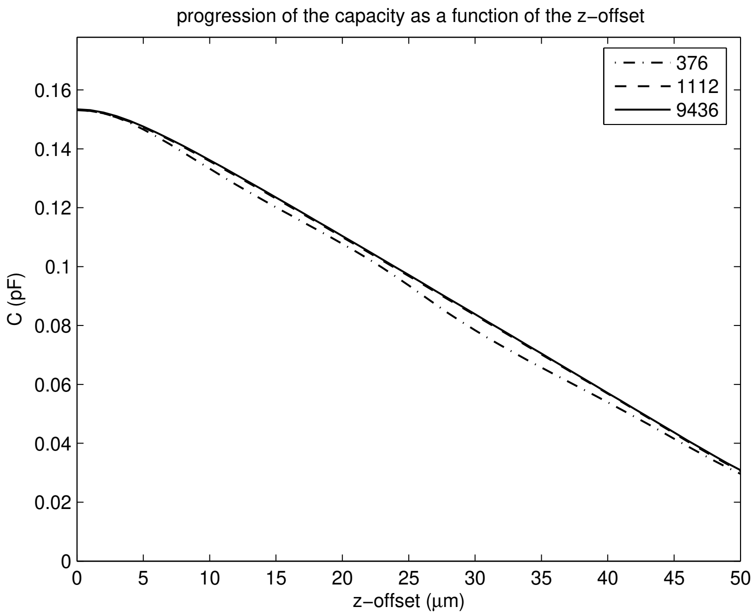

Figure 4: Capacity for centered transducers and $\nu = 1$ (piecewise linear functions).

are needed to discretize the thin structures with regular elements.

The more challenging task are computations when the distance between the fingers is small compared to the thickness of the fingers (see Fig. 5), where the gap is only $0.1\mu m$.

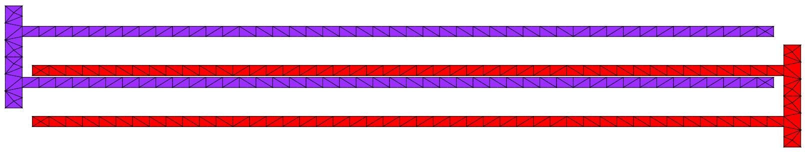

Figure 5: Minimal distance between the fingers: $0.1\mu m$.

Although the geometry of each finger seems to be simple some effort is needed to resolve the different length scales in particular when the distance between the fingers becomes small. Hence the number of boundary elements needed in the discretization process to ensure an efficient accuracy is quite huge. Therefore, a standard Galerkin boundary element method yielding dense stiffness matrices is not applicable anymore. There is a need to use fast boundary element methods such as the Fast Multipole Method (FMM) [6], the panel clustering algorithm [8], algebraic approximation methods like the Adaptive Cross Approximation [1, 15] and hierarchical matrices [7], or wavelets [17].

Before discussing an application of the fast multipole method to solve the linear system $V_h^\nu \underline{t}^\nu = \underline{f}^\nu$, we have to consider an appropriate iterative solution method. Since the stiffness matrix V_h^ν is symmetric and positive definite, we may apply the conjugate gradient scheme as an iterative solver. Since the spectral condition number $\kappa_2(V_h^\nu)$ behaves like $\mathcal{O}(h^{-1})$ a suitable preconditioner is needed. In particular, we use the Artifical Multilevel Boundary Element Preconditioner $C_{V,h}^{-1}$ introduced in [18]. It is a BPX–like preconditioner [2] build on an artifical hierarchy of trial spaces. Let $Z_h = Z_J \subset S_h^0(\Gamma)$ be the space of piecewise constant basis functions. Further, let a series of nested trial spaces Z_j

$$Z_0 \subset Z_1 \subset \ldots \subset Z_J = Z_h$$

exit with mesh sizes $h_j = \frac{1}{2}h_{j-1}$. The multilevel operator A^s is defined for $s \in \mathbb{R}$ as

$$A^s = \sum_{j=0}^{J} h_j^{-2s}(Q_j - Q_{j-1}),$$

where Q_j is the $L_2(\Gamma)$ projection onto Z_j by

$$\langle Q_j w, \tau\rangle_\Gamma = \langle w, \tau\rangle_\Gamma \qquad \text{for all } \tau \in Z_j, j = 0, \ldots, J,$$

for $w \in L_2(\Gamma)$ and $Q_{-1} = 0$. Due to the spectral equivalence inequalities [13]

$$c_1\|w\|^2_{H^{-1/2}(\Gamma)} \le \langle A^{-1/2}w, w\rangle_\Gamma \le c_2 J^2 \|w\|^2_{H^{-1/2}(\Gamma)}$$

for all $w \in Z_J$, the multilevel operator $A^{-1/2}$ can be used as a preconditioner of the single layer potential. Since the single layer potential is elliptic and bounded with constants c_1^V and c_2^V independent of h, the spectral equivalence inequalities

$$\frac{c_1^V}{J^2 c_2}\langle A^{-1/2}w, w\rangle_\Gamma \le \langle Vw, w\rangle_\Gamma \le \frac{c_2^V}{c_1}\langle A^{-1/2}w, w\rangle_\Gamma \tag{8}$$

hold for all $w \in H^{-1/2}(\Gamma)$. Note that $A^{-1/2}A^{1/2} = I$ holds. The corresponding preconditioning matrix $C_{V,h}^{-1}$ is given by

$$C_{V,h}^{-1} = M_h^{-1} A_h^{1/2} M_h^{-1}. \tag{9}$$

The entries of the used matrices are defined by

$$A_h^{1/2}[\ell, k] = \langle A^{1/2}\psi_k^0, \psi_\ell^0\rangle_\Gamma, \quad M_h[\ell, k] = \langle \psi_k^0, \psi_\ell^0\rangle_{L_2(\Gamma)}.$$

Due to the exact representation of the basis functions ψ_k^0 of Z_k by the basis functions of the finer trial space Z_{k+1}, any discrete function $z_h^k \in Z_k$ can be writen in terms of the basis functions of Z_{k+1} as

$$\underline{z}^{k+1} = R_{k,k+1}\underline{z}^k$$

where $R_{k,k+1} \in \mathbb{R}^{n_{k+1}\times n_k}$. A spectrally equivalent realization [19] of $\underline{v} = C_{V,h}^{-1}\underline{r}$ is given by

$$\underline{v} = \sum_{k=0}^{J} h_k^{-1} R_k R_k^\top \underline{r},$$

where $R_J = I$ and $R_k = R_{k+1} R_{k,k+1}$ for $0 \le k < J$.

This kind of preconditioning has been used in [4] based on a nested sequence of boundary element spaces constructed by geometrical refinement of the boundary elements. Here, we use the cluster hierarchy of the fast multipole method to construct the sequence of nested boundary element spaces due to the idea in [18]. The clusters ω_i^j on level $j \le L$ of the cluster tree with cluster depth L define the fictitious boundary elements τ_i^j of the coarser trial spaces Z_j for $j < J = L + 1$.

This construction is restricted to piecewise constant basis functions. For piecewise linear and discontinuous basis functions, we use an piecewise constant approximation on a refined boundary element mesh to define a preconditioner.

Next, we describe an application of the fast multipole method to the single layer potential based on the original version in [5, 6]. Detailed descriptions of the fast multipole method and further references can be found in [12]. A matrix times vector multiplication $\underline{w} = V_h^\nu \underline{t}$ of the single layer potential can be written component-wise

$$w_\ell = \sum_{k=1}^{N} V_h^\nu[\ell, k] t_k = \sum_{k=1}^{N} \frac{t_k}{4\pi} \int_\Gamma \psi_\ell^\nu(x) \int_\Gamma \frac{\psi_k^\nu(y)}{|x - y|} ds_y ds_x \tag{10}$$

for all $\ell = 1, \dots, N$. The effort for setting up this matrix and for one matrix times vector multiplication is quadratic in N. If we could write the kernel $k(x, y) = |x - y|^{-1}$ as a product $f(x) \cdot g(y)$ with a separation of variables, this effort would be reduced to linear complexity. Unfortunately, this separation of variables is only possible by using a series expansion of the kernel. In the case of the Laplacian, spherical harmonics [9] are more suitable to use than a Taylor series. Therefore, an appropriate approximation $k_p(x, y)$ of the kernel $k(x, y)$ is given by

$$k_p(x, y) = \sum_{n=0}^{p} \sum_{m=-n}^{n} \overline{S_n^m}(y) R_n^m(x) \qquad \text{for } |x| < |y|, \tag{11}$$

using modified spherical harmonics [14, 20, 21]

$$\begin{aligned} R_n^{\pm m}(x) &= \frac{1}{(n+m)!} \frac{d^m}{du^m} P_n(u)\big|_{u=\widehat{x}_3} (\widehat{x}_1 \pm i\widehat{x}_2)^m \, |x|^n \,, \\ S_n^{\pm m}(y) &= (n-m)! \frac{d^m}{du^m} P_n(u)\big|_{u=\widehat{y}_3} (\widehat{y}_1 \pm i\widehat{y}_2)^m \frac{1}{|y|^{n+1}} \end{aligned}$$

for $m \ge 0$ and $\widehat{x} = x/|x|$. P_n denote the Legendre polynomials. Since this degenerated kernel is not valid everywhere, it is only used when the boundary element τ_k is sufficiently far away from the evaluation element τ_ℓ. Therefore we distinguish in a far-field $\mathrm{FF}(\ell)$ and a near-field $\mathrm{NF}(\ell)$ to realize the matrix times vector multiplication for $\ell = 1, \dots, N$ as

$$\widetilde{w}_\ell = \sum_{k \in \mathrm{NF}(\ell)} V_h[\ell, k] t_k + \frac{1}{4\pi} \sum_{n=0}^{p} \sum_{m=-n}^{n} M_n^m(O, \ell) \widetilde{L}_n^m(\mathrm{FF}(\ell)). \tag{12}$$

The coefficients

$$M_n^m(O,\ell) = \int_\Gamma \psi_\ell^\nu(x) R_n^m(x) ds_x$$

can be evaluated by a numerical quadrature rule or exactly for plain triangles [10, 11] with respect to a local origin O. Note, the support of a basis function ψ_ℓ^ν is just one triangle. If the coefficients

$$\widetilde{L}_n^m(\mathrm{FF}(\ell)) = \sum_{k \in \mathrm{FF}(\ell)} t_k \int_\Gamma \psi_k^\nu(y) \overline{S_n^m}(y) ds_y \tag{13}$$

can be computed for $n = 0, \dots, p, m = -n, \dots, n$ efficiently, we will have a fast realization of the matrix times vector multiplication by (12). The difficulties are that the coefficients $\widetilde{L}_n^m(\mathrm{FF}(\ell))$ depend on the different far-fields $\mathrm{FF}(\ell)$. So a hierarchical structure is built on the boundary elements τ_k. All boundary elements $\{\tau_k\}_{k=1}^n$ are positioned in a cube containing the whole domain Ω and form the cluster ω_1^0 of the coarsest level 0. For any cluster ω_i^λ the corresponding cube is refined in eight similar smaller cubes. The triangles of the cluster ω_i^λ are assigned to these smaller cubes and form up to eight new clusters $\omega_j^{\lambda+1}$ as sons of the cluster ω_i^λ. This refinement is carried out up to a maximal level L. Now we can concretize the definitions of the near-field and the far-field. A cluster ω_i^λ is said to be in the near-field of a cluster ω_j^λ of the same level λ, if the condition

$$\mathrm{dist}\,\{C_i^\lambda, C_j^\lambda\} \le (d+1)\max\{r_i^\lambda, r_j^\lambda\} \tag{14}$$

is fulfilled. C_i^λ denotes the midpoint of the cube of cluster ω_i^λ, d the nearfield parameter and r_i^λ the corresponding radius of the cluster, i.e. $r_i^\lambda = \sup_{x\in\omega_i^\lambda} \left|x - C_i^\lambda\right|$. This definition is transferred to the boundary elements τ_k via the leafs of the cluster tree:

$$\begin{aligned} \mathrm{NF}(\ell) \;&:=\; \{k : 1 \le k \le N \text{ and (14) is valid for the} \\ &\qquad \text{clusters } \omega_i^L \text{ of } \tau_k \text{ and } \omega_j^L \text{ of } \tau_\ell.\}\,, \\ \mathrm{FF}(\ell) \;&:=\; \{1, \dots, N\} \setminus \mathrm{NF}(\ell). \end{aligned}$$

Now this cluster hierarchy is used to evaluate the coefficients $\widetilde{L}_n^m(\mathrm{FF}(\ell))$. First, the multipole coefficients

$$\widetilde{M}_n^m(C_j^L, P_j^L) = \sum_{\tau_k \in \omega_j^L} \int_{\tau_k} t_h(x) R_n^m(x) ds_x$$

are evaluated for all clusters ω_j^L of the finest cluster level L. $P_j^\lambda := \{k : \tau_k \in \omega_j^\lambda\}$ denotes the set of all boundary elements τ_k of the cluster ω_j^λ. Then the coefficients $\widetilde{M}_n^m$ are used to compute the multipole coefficients of all coarser levels by means of the translation

$$\begin{aligned} \widetilde{M}_n^m(C_j^\lambda, P_j^\lambda) \;&=\; \sum_{\omega_i^{\lambda+1} \in \mathrm{Sons}(\omega_j^\lambda)} \sum_{s=0}^{n} \sum_{t=-s}^{s} R_s^t(\overrightarrow{C_j^\lambda C_i^{\lambda+1}}) \\ &\qquad \cdot \widetilde{M}_{n-s}^{m-t}(C_i^{\lambda+1}, P_i^{\lambda+1}). \end{aligned}$$

Based on these multipole coefficients of a cluster ω_j^λ, the local coefficients of another cluster ω_i^λ in the far-field of ω_j^λ are determined by the conversion

$$\widetilde{L}_n^m(C_i^\lambda, P_j^\lambda) = \sum_{s=0}^{\infty} \sum_{t=-s}^{s} (-1)^n \overline{S_{n+s}^{m+t}}(\overrightarrow{C_j^\lambda C_i^\lambda}) \widetilde{M}_s^t(C_j^\lambda, P_j^\lambda).$$

These conversions are only executed on the coarsest level on which the admissibility condition is satisfied. The local coefficients are summed up for each cluster ω_i^λ. Further, they are translated from each cluster ω_i^λ to its sons $\omega_j^{\lambda+1}$ by

$$\begin{aligned}\widetilde{L}_n^m(C_j^{\lambda+1}, \mathrm{FF}(\omega_i^\lambda)) \quad = \quad & \sum_{s=n}^{p} \sum_{t=-s}^{s} R_{s-n}^{t-m}(\overrightarrow{C_i^\lambda C_j^{\lambda+1}}) \\ & \cdot \widetilde{L}_s^t(C_i^\lambda, \mathrm{FF}(\omega_i^\lambda)).\end{aligned}$$

The sum of all coefficients $\widetilde{L}_n^m(C_j^L, \cdot)$ gives the coefficients $\widetilde{L}_n^m(\mathrm{FF}(\ell))$ needed for the matrix times vector product (12), where ω_j^L is the cluster containing τ_ℓ. Note, the computation of all the coefficients has to be redone for each matrix times vector multiplication.

A detailed analysis [12] of the method and numerical tests show that the fast multipole approximation preserves the main properties of the matrix V_h^ν. For example, the fast multipole boundary element method provides the same asymptotic convergence rate as the standard boundary element method for the approximation t_h of the solution $t_{|\Gamma}$.

Due to this consistency analysis the expansion degree has to be chosen as $p \sim \log n$ for a fixed parameter d. This leads to a total effort of $\mathcal{O}(n \log^2 n)$ for a matrix times vector multiplication as well as the memory requirements.

4 Numerical Studies

We now consider the characteristic curves of the computed capacitances in Fig. 6 obtained for the configuration of Fig. 5 with the small gap of 0.1 μm. The computations have been executed for steps of 1 μm in z–direction. The coarse boundary element meshes give a bad approximation of the characteristic curves. If we take a look at a good approximation t_h, we will see a huge jump on each of finger structures at the height where the other finger structure ends. If a new row of boundary elements starts at the actual z–offset, we will get a better approximation by the coarse boundary element meshes. This explains the peaks in the approximations of the characteristic curves by the piecewise constant trial functions on the coarse boundary element grids in Fig. 6. The approximations of the characteristic curve are worse than for the centered configuration, as the boundary element mesh has to resolve the small distance between the two domains in some way. For the finer boundary element meshes of 37744 and 150976 boundary elements we obtain good approximations of the characteristic curve.

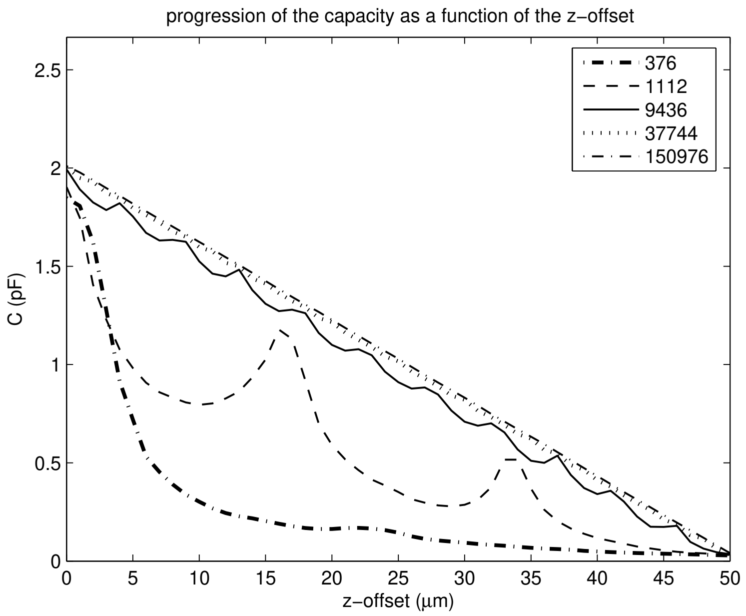

Figure 6: Capacity for transducers with small gap and $\nu = 0$.

If we use piecewise linear and discontinuous trial functions, we get better results as shown in Fig. 7 for the same boundary element meshes due to the higher number of degrees of freedom and the possibly higher convergence rate in (7).

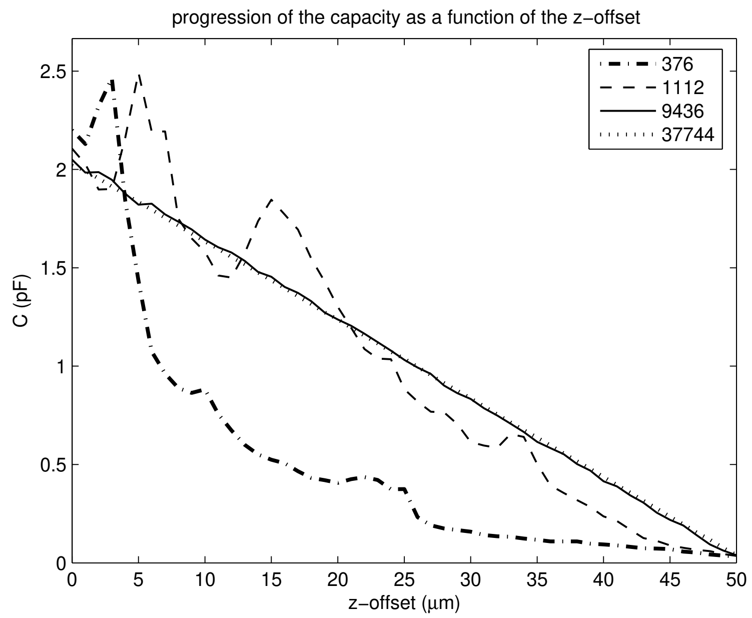

Figure 7: Capacity for transducers with small gap and $\nu = 1$.

The use of piecewise linear and discontinuous trial functions leads to a higher number of unknowns and larger matrices. The number of entries in a standard boundary element method is increased by a factor of nine. Therefore their use is more expensive than the one of the piecewise constant basis functions. In Fig. 8 we compare the characteristic curves obtained by the piecewise constant trial functions with 37744 and 150976 boundary elements to the characteristic curves of piecewise linear and discontinuous trial functions with 37744 boundary elements.

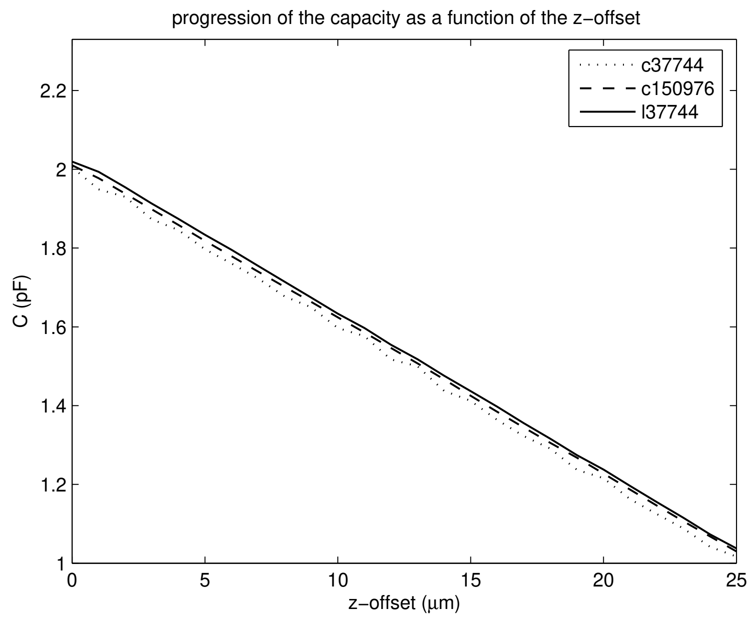

Figure 8: Comparison of constant and linear trial functions.

In the zoom, the solid line of the characteristic curve of the piecewise linear basis functions is at least a better approximation than the dotted one of the piecewise constant trial functions on the same boundary element mesh. It is hard to decide whether the approximation by the piecewise linear basis functions is better than the one of the piecewise constant trial functions on the refined mesh.

Next, we will comment on the numbers of iterations and computational times needed for this numerical examples. The computations have been executed on an Linux PC with an INTEL 3.066 GHz processor and 1GB of RAM. We have selected values of the z–offsets of 0 μm, 25 μm and 50 μm. In Table 1 the number of iterations and the computational times for the centered configuration are listed.

We do not show results of the solution process without preconditioning, but the used artificial multilevel preconditioner reduces the iteration numbers and the computational times significantly. The bad quality of the two coarsest boundary element meshes influences the quality of the preconditioning. These values are dropped in the Tables, since they might give a wrong idea of the asymptotic behavior. Therefore, only the values of the regular

DoF	$0\mu m$ Iter	$0\mu m$ sec	$25\mu m$ Iter	$25\mu m$ sec	$50\mu m$ Iter	$50\mu m$ sec
piecewise constant basis functions						
9436	53	82	52	71	47	51
37744	58	419	60	347	54	246
150976	64	2018	66	1702	58	1361
piecewise linear basis functions						
28308	109	349	106	295	96	212
113232	113	1377	113	1112	102	796

Table 1: computational efforts for the centered configuration

mesh and its uniform refinements are considered. There is a slight logarithmic grow of the number of iterations due to the increase of the number of unknowns, as expected from theory. The number of iterations of the piecewise linear and discontinuous trial functions are higher, since the preconditioner is only applied to a piecewise constant approximation on a finer grid. The increase of the computational times is in good agreement with the $\mathcal{O}(n \log^2 n)$ asymptotic of the fast multipole method and the logarithmic grows of the iteration numbers. The piecewise linear and discontinuous trial functions benefit a lot from the use of the fast multipole method. Using a fast multipole method, only the near-field part is increased by a factor of nine. In the far-field part the three local basis functions only effect the setup of the multipole coefficients and the evaluation of the local expansions by a factor of three. The rest, the computation of the other coefficients in the fast multipole method, can be done at once. This effect can be seen in the computational times.

We now go back to the more interesting case of the small gap between the two finger structures, where we have compared the quality of the different approximations. In Table 2 the numbers of iterations and the computational times are shown.

DoF	$0\mu m$ Iter	$0\mu m$ sec	$25\mu m$ Iter	$25\mu m$ sec	$50\mu m$ Iter	$50\mu m$ sec
piecewise constant basis functions						
9436	106	97	88	82	48	54
37744	142	567	80	359	54	232
150976	159	2820	78	1701	60	1327
piecewise linear basis functions						
28308	180	394	166	334	105	265
113232	152	1351	133	1122	108	782

Table 2: Computational efforts for a small gap

Compared to the values for the centered configuration in Table 1, the numbers of iterations are increased. This can be explained by the higher complexity due to the small gap, which leads to worse ellipticity and boundedness constants of the single layer potentials. These constants worsen the condition number of the considered problem. This effect is decreasing with increasing z–offset, such that there is almost no difference in the iteration numbers of the centered configuration and the setting with a small gap in the case of a z–offset of 50 μm. The increasing number of iterations leads to larger computational times. There are also small differences in the computational times due to changes in the cluster tree of the fast multipole method. In some cases the iteration number is decreasing while the number of boundary elements is increasing. This is due to the better resolution of the complexity of the problem by the finer mesh. This effect is also observed for the coarse meshes in the centered configuration.

	centered			small gap		
DoF	$0\mu m$	$25\mu m$	$50\mu m$	$0\mu m$	$25\mu m$	$50\mu m$
piecewise constant basis functions						
9436	46	43	37	48	45	38
37744	169	157	139	163	157	142
150976	731	674	631	739	698	642
piecewise linear basis functions						
28308	254	218	168	276	245	179
113232	812	708	543	812	755	614

Table 3: Memory requirements (MB)

In Table 3, we compare the memory requirements for the considered configurations and basis functions. For piecewise constant basis functions, the memory requirements increase almost linearly with the increasing number of boundary elements as expected from theory. The compression of the number of near-field matrix entries gets better with increasing z–offset, since the near-fields get smaller. Therefore the memory requirements are reduced. In the case of the small cap between the two structures, the near-fields get a little bit larger and the memory requirements increase. The size of the near-field matrix of the piecewise linear and discontinuous basis functions is nine times the size of the one of the piecewise constant basis functions. The memory requirements of the far-field part are the same for both kind of basis functions. Therefore the observed increase of the memory requirements is smaller than expected asymptotically.

Overall, it seems that the piecewise linear and discontinuous trial functions give an approximation, which is almost as good as the one of the piecewise constant trial functions on the refined mesh, at lower costs computational cost and at about the same memory requirements.

5 Conclusions and Further Remarks

We have presented an efficient computational scheme for the evaluation of electric capacities within micromechanical transducers. The arising algebraic system of equation obtained by a Galerkin BEM is efficiently solved by a CG-method with an multilevel BE-Preconditioner and an appropriate fast multipole algorithm for the matrix-vector operations within the CG-iterations. The numerical case study demonstrated the robustness of the developed numerical method with respect to the number of iterations and the complexity of the problem.

Acknowledgement

This work has been supported by the German Research Foundation 'Deutsche Forschungsgemeinschaft (DFG)' under the grant SFB 404 'Multifield Problems in Continuum Mechanics'. Part of the work was done while the first two author stayed at the Johann Radon Institute for Computational and Applied Mathematics (RICAM) on the occasion of the Special Radon Semester 2005 in Linz. The support of the RICAM is gratefully acknowledged.

References

[1] M. Bebendorf, S. Rjasanow: Adaptive low–rank approximation of collocation matrices. Computing 70 (2003) 1–24.

[2] J. H. Bramble, J. E. Pasciak, J. Xu: Parallel multilevel preconditioners. Math. Comput. 55 (1990) 1–22.

[3] A. Buchau, M.R. Rucker: Preconditioned Fast Adaptive Multipole Boundary-Element Method. IEEE Trans. on Magnetics, 38(2) (2002) 461–464.

[4] S. A. Funken, E. P. Stephan: The BPX preconditioner for the single layer potential operator. Appl. Anal. 67 (1997) 327–340.

[5] L. Greengard: The Rapid Evaluation of Potential Fields in Particle Systems. The MIT Press, 1987.

[6] L. Greengard, V. Rokhlin: A fast algorithm for particle simulations. J. Comput. Phys. 73 (1987) 325–348.

[7] W. Hackbusch: A sparse matrix arithmetic based on $\mathcal{H}$–matrices. I. Introduction to $\mathcal{H}$–matrices. Computing 62 (1999) 89–108.

[8] W. Hackbusch, Z. P. Nowak: On the fast matrix multiplication in the boundary element method by panel clustering. Numer. Math. 54 (1989) 463–491.

[9] E. W. Hobson: The theory of spherical and ellipsoidal harmonics. Cambridge: Univ. Press., 1931.

[10] K. Nabors, F. T. Korsmeyer, F. T. Leighton, J. White: Preconditioned, adaptive, multipole-accelerated iterative methods for three-dimensional first-kind integral equations of potential theory. SIAM J. Sci. Comput. 15 (1994) 713–735.

[11] J. N. Newman: Distributions of sources and normal dipoles over a quadrilateral panel. Journal of Engineering Mathematics 20 (1996) 113–126.

[12] G. Of, O. Steinbach, W. L. Wendland: The fast multipole method for the symmetric boundary integral formulation. IMA J. Numerical Analysis 26 (2006) 272–296.

[13] P. Oswald: Multilevel norms for $H^{-1/2}$. Computing 61 (1998) 235–255.

[14] J. M. Perez-Jorda, W. Yang: A concise redefinition of the solid spherical harmonics and its use in the fast multipole methods, J. Chem. Phys. 104 (1996) 8003–8006.

[15] S. Rjasanow, O. Steinbach: The Fast Solution of Boundary Integral Equations. Mathematical and Analytical Techniques with Applications to Engineering. Springer, New York, 2007.

[16] V. Rokhlin: Rapid solution of integral equations of classical potential theory. J. Comput. Phys. 60 (1985) 187–207.

[17] R. Schneider: Multiskalen– und Wavelet–Matrixkompression: Analysisbasierte Methoden zur effizienten Lösung grosser vollbesetzter Gleichungssysteme. Advances in Numerical Mathematics. B. G. Teubner, Stuttgart, 1998.

[18] O. Steinbach: Artificial multilevel boundary element preconditiones. Proc. Appl. Math. Mech. 3 (2003) 539–542.

[19] O. Steinbach: Numerische Näherungsverfahren für elliptische Randwertprobleme. Finite Elemente und Randelemente. B. G. Teubner, Stuttgart, Leipzig, Wiesbaden, 2003.

[20] Ch. A. White, M. Head–Gordon: Derivation and efficient implementation of the fast multipole method. J. Chem. Phys. 101 (1994) 6593–6605.

[21] K. Yoshida: Applications of Fast Multipole Method to Boundary Integral Equation Method, Kyoto University, 2001.

Erschienene Preprints ab Nummer 2005/1

2005/1	O. Steinbach	Numerische Mathematik 1. Vorlesungsskript.
2005/2	O. Steinbach	Technische Numerik. Vorlesungsskript.
2005/3	U. Langer G. Of O. Steinbach W. Zulehner	Inexact Fast Multipole Boundary Element Tearing and Interconnecting Methods
2005/4	U. Langer G. Of O. Steinbach W. Zulehner	Inexact Data–Sparse Boundary Element Tearing and Interconnecting Methods
2005/5	U. Langer O. Steinbach W. L. Wendland	Fast Boundary Element Methods in Industrial Applications Söllerhaus Workshop, 25.–28.9.2005, Book of Abstracts.
2005/6	U. Langer A. Pohoata O. Steinbach	Dual–Primal Boundary Element Tearing and Interconnecting Methods
2005/7	O. Steinbach (ed.)	Jahresbericht 2004/2005
2006/1	S. Engleder O. Steinbach	Modified Boundary Integral Formulations for the Helmholtz Equation.
2006/2	O. Steinbach	2nd Austrian Numerical Analysis Day. Book of Abstracts.
2006/3	B. Muth G. Of P. Eberhard O. Steinbach	Collision Detection for Complicated Polyhedra Using the Fast Multipole Method of Ray Crossing
2006/4	G. Of B. Schneider	Numerical Tests for the Recovery of the Gravity Field by Fast Boundary Element Methods
2006/5	U. Langer O. Steinbach W. L. Wendland	4th Workshop on Fast Boundary Element Methods in Industrial Applications. Book of Abstracts.
2006/6	O. Steinbach (ed.)	Jahresbericht 2005/2006
2006/7	G. Of	The All–floating BETI Method: Numerical Results
2006/8	P. Urthaler G. Of O. Steinbach	Automatische Positionierung von FEM–Netzen
2006/9	O. Steinbach	Challenges and Applications of Boundary Element Domain Decomposition Methods
2006/10	S. Engleder	Stabilisierte Randintegralgleichungen für äussere Randwertprobleme der Helmholtz-Gleichung
2007/1	M. Windisch	Modifizierte Randintegralgleichungen für elektromagnetische Streuprobleme
2007/2	M. Kaltenbacher G. Of O. Steinbach	Fast Multipole Boundary Element Method for Electrostatic Field Computations